Proceedings of the ASME 2013 Dynamic Systems and Control Conference
DSCC2013
October 21-23, 2013, Palo Alto, California, USA

DSCC2013-3935

MAXIMUM POWER ESTIMATION OF LITHIUM-ION BATTERIES ACCOUNTING FOR THERMAL AND ELECTRICAL CONSTRAINTS

Youngki Kim*, Shankar Mohan, Jason B. Siegel and Anna G. Stefanopoulou
University of Michigan
Ann Arbor, Michigan 48109
Email: {youngki,elemsn,sigeljb,annastef}@umich.edu

ABSTRACT

Enforcement of constraints on the maximum deliverable power is essential to protect lithium-ion batteries from overcharge/discharge and overheating. This paper develops an algorithm to address the often overlooked temperature constraint in determining the power capability of battery systems. A prior knowledge of power capability provides dynamic constraints on currents and affords an additional control authority on the temperature of batteries. Power capability is estimated using a lumped electro-thermal model for cylindrical cells that has been validated over a wide range of operating conditions. The time scale separation between electrical and thermal systems is exploited in addressing the temperature constraint independent of voltage and state-of-charge (SOC) limits. Limiting currents and hence power capability are determined by a model-inversion technique, termed Algebraic Propagation (AP). Simulations are performed using realistic depleting currents to demonstrate the effectiveness of the proposed method.

NOMENCLATURE

c_p Heat capacity of a battery
h Convection coefficient
n Number of electrons involved in the electrode reaction
A_b Surface area of a battery
C Capacitance
F Faraday's constant
I Current
M Mass of a battery
C_b Capacity of a battery
R Resistance
S Entropy
T Bulk temperature of a battery
T_∞ Ambient temperature
V Terminal voltage
V_{oc} Open circuit voltage of a battery

*Address all correspondence to this author.

1 INTRODUCTION

Lithium-ion batteries have been used as an energy storage system in numerous applications such as laptop computers, satellites, mobile robots, and electrified vehicles due to their superior performance such as high power and energy density [1]. However, the lithium-ion battery cycle life or capacity decreases considerably during operations at high temperature due to irreversible chemical reactions [2]. If the battery temperature is not monitored and controlled, the battery could have a thermal runaway with the possible risk of explosion [3,4].

To avoid aging and capacity loss, battery manufacturers specify voltage and current limits and recommended operating temperature ranges. Thus, limits on the operating temperature of lithium-ion batteries must be enforced to ensure safe and reliable operation of the battery. Temperature regulation of battery packs can be achieved by utilizing active thermal management systems or limiting the peak current drawn from the pack. These strategies increase the rate of heat rejection or limit the rate of internal heat generation respectively [5]. Since lithium-ion batteries for applications such as laptop computers, satellites and mobile robots usually have limited cooling, it is critical to control the discharge current of batteries so that operating temperatures do not exceed the maximum value. Traditionally, thermostatic or proportional-integral-derivative (PID) controllers are used to limit current or power drawn from the battery when the measured temperature exceed the predefined limits. Calibrating thermostatic thresholds, dead-bands and PID gains and integrat-

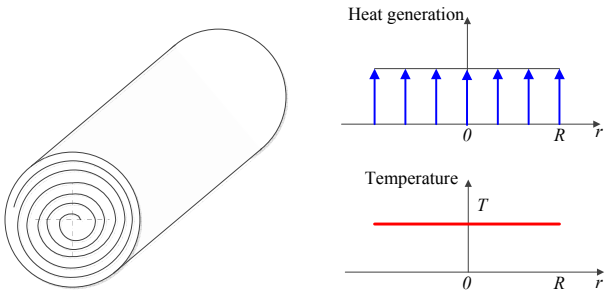

Figure 1. SCHEMATIC OF A CYLINDRICAL CELL

ing them with the overall power allocation strategies in battery management systems is a non-trivial problem.

The power capability of a battery cell in the context of this paper refers to the constant power that can be drawn safely from the cell over a finite window of time. Information on the power capability is useful in making decisions as part of a supervisory controller. Model-based methods to estimate power capability in real time have been addressed in works such as [6–8], wherein, algorithms accounting for electrical constraints such as terminal voltage and battery SOC are developed. This paper improves upon the state-of-the-art in that it accounts for both thermal and electrical constraints. Specifically, a simple, computationally efficient, model-based method to calculate the maximum current rate/power capability is proposed.

This paper is organized as follows. Section 2 presents a thermal model incorporating information on entropy change in addition to joule heating and convection phenomena. Then, a simple equivalent circuit electrical model is presented in Section 3 for the electrical dynamics of the battery. In Section 4, a model-based maximum power estimation method is proposed to determine the maximum current/power capability over a fixed horizon considering both thermal and electrical constraints independently. Simulation results are discussed in Section 5 and conclusions are drawn in Section 6.

2 THERMAL MODEL

A cylindrical Li-ion battery cell, e-Moli ICR18650J 2.3 Ah, is considered in this study. This battery is fabricated by rolling a stack of layered thin sheets comprised of a Lithium Cobalt Oxide ($LiCoO_2$) cathode, a separator, and a graphitic anode in a manner similar to the schematic in Fig. 1. Uniform heat generation along the radial direction is assumed, which is a standard assumption [9, 10]. Lumped parameters are used so that material properties such as thermal conductivity, density and specific heat capacity are assumed to be constant in a homogeneous and isotropic body. Since the thermal conductivity is one or two orders of magnitude higher in the axial direction than in the radial direction, the temperature distribution in the axial direction will be more uniform [11, 12]. The Biot number of the battery cell with natural convection is small ($Bi \ll 0.1$), suggesting that the heat transfer at the surface is much smaller than the internal heat transfer by conduction. Hence, no significant temperature gradient inside the cell is expected.

Under the above assumptions, the energy balance equation in the cell can be described by one bulk cell temperature [13]:

$$\begin{aligned} Mc_p \frac{dT}{dt} &= Q_{\text{gen}} + Q_{\text{rev}} + Q_{\text{rej}} \\ Q_{\text{gen}} &= I^2 R_e \\ Q_{\text{rev}} &= -IT\frac{\Delta S}{nF} \\ Q_{\text{rej}} &= A_b h(T_\infty - T) \end{aligned} \tag{1}$$

where Q_{gen}, Q_{ref}, and Q_{rej} represent joule heating, entropic heat generation, and heat transfer through convection respectively. The internal resistance R_e lumps ohmic, activation, diffusion polarization resistances. In the chosen sign convention, a positive current discharges the battery.

The energy balance equation is described in the state space representation:

$$\dot{x}_\theta = \alpha x_\theta + \beta x_\theta u + \gamma u^2 + \eta \tag{2}$$

where the state and input of the system are $x_\theta = T$ and $u = I$, respectively. The parameters are defined by

$$\alpha = \frac{-A_b h}{Mc_p},\ \beta = \frac{-1}{Mc_p}\frac{\Delta S}{nF},\ \gamma = \frac{R_e}{Mc_p},\ \eta = \frac{A_b h T_\infty}{Mc_p}. \tag{3}$$

This nonlinear thermal dynamic model is used to predict the temporal evolution of temperature and to formulate a current limiting strategy in Section 4.

2.1 Entropy Measurement

The contribution of the entropy change ΔS to the total heat generation in a $LiCoO_2/LiC_6$ cell is significant at low current rates [14]. Therefore, it is important to determine the entropy change of the battery cell for predicting the temperature of a battery accurately. The entropy change can be identified by using the change in the open circuit voltage, V_{oc}, as a function of temperature [13] according to Eq. (4)

$$\Delta S = nF\frac{\partial V_{OC}}{\partial T}. \tag{4}$$

Figures 2(a) and (b) illustrate the experimental set-up in this study for characterizing entropy change. The battery is fully charged at a rate of C/20[1] at 25 ^{o}C using a Constant Current

[1] A 1C current corresponds to the magnitude of current that discharges/charges the cell completely in one hour.

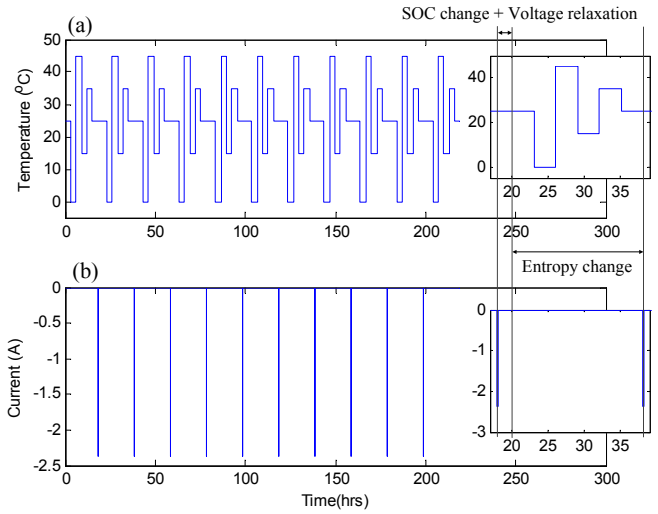

Figure 2. EXPERIMENTAL DESIGN TO ESTIMATE ENTROPY CHANGE OF THE BATTERY: (a) AMBIENT TEMPERATURE PROFILE; (b) CURRENT PROFILE

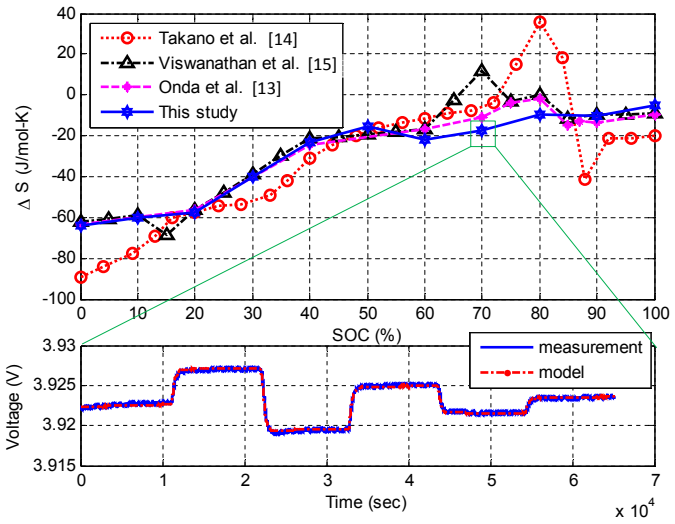

Figure 3. MEASURED ENTROPY CHANGE: (a) COMPARISON WITH LITERATURE VALUES; (b) MEASURED AND SIMULATED OPEN CIRCUIT VOLTAGES AT 80% SOC

Constant Voltage protocol with a cutoff current rate of C/100. The temperature in the thermal chamber is controlled as shown in Fig. 2(a). The battery cell is allowed to rest for three hours at each temperature to equilibrate. To change the SOC of the battery by 10%, a current at a rate of 1C is applied to the battery for six minutes at 25 ^{o}C that is followed by two hours of rest for charge equilibrium.

Figure 3(a) shows the entropy change of the $LiCoO_2/LiC_6$ battery cell in this study and compares the values from the literature [13–15]. It is observed that the entropy change in the SOC range of 60% to 80% is estimated differently in different studies. Clearly some batteries in these studies have endothermic process while the others have exothermic process during battery discharge. In particular, the battery cell in this study does not have endothermic process, leading to a higher total heat generation during battery discharge than batteries in [13–15]. Figure 3(b) compares measured and predicted open circuit voltages of the battery at 70% SOC, providing that the measured entropy change of the battery is reasonably accurate.

2.2 Thermal Parametrization

To predict the temperature of the cell, thermal parameters, namely heat capacity c_p and convection coefficient h are to be parameterized. Parameterization is performed as follows – a current profile such as the one presented in Fig. 4(a) is applied to the battery cell placed in a temperature controlled chamber and its surface temperature, terminal voltage and current are measured as shown in Fig. 4(a)–(c). The time constant of the thermal system α is approximated from the relaxation data following the initial constant current phase. Imposing the relation between h and c_p in Eq. (3) as an equality constraint, the parameterization is formulated in the form of optimization problem by using data collected during discharge operation as follows

$$\begin{aligned} \min\ & J = ||\hat{T}(c_p) - T|| \\ \text{subject to}\ & hA_b + \alpha M c_p = 0. \end{aligned}$$

where T and $\hat{T}$ are measured and predicted temperatures respectively.

The optimization problem is implemented and solved in

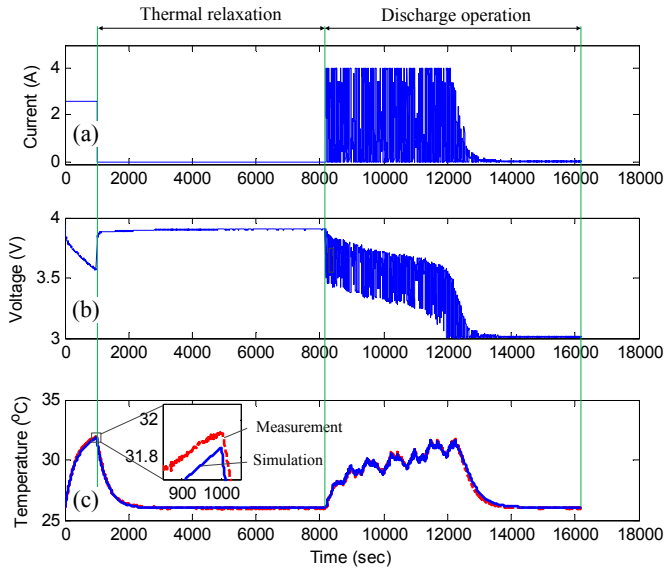

Figure 4. MEASUREMENT DATA USED FOR THERMAL PARAMETRIZATION: (a) CURRENT; (b) VOLTAGE; (c) TEMPERATURE

MALTAB using the built-in function *fmincon* [16]. The heat capacity of SONY 18650 cells, which have similar chemistries to the e-Moli ICR 18650 cells under consideration, can be found in open literature [11]. It is found that the values for heat capacity c_p lie between 836 and 1280 J/kg/K. In this study, c_p=1000 J/kg/K is chosen as an initial value to the optimization problem. The identified parameters c_p and h are 1248 J/kg/K and 42.9 W/m^2/K respectively. As demonstrated in Fig. 4(c), the parameterized thermal model can provide accurate prediction of the temperature during battery operation.

3 ELECTRICAL MODEL

In control applications, the equivalent circuit model is favored owing to its simplicity and has been shown to be reasonably capable of emulating the dynamics of a battery cell [17, 18]. In this study, the equivalent circuit model is used and the electrical system is described by

$$\begin{aligned} S\dot{O}C &= -\frac{I}{C_b}, \\ \dot{V}_i &= -\frac{1}{R_i C_i} V_i + \frac{1}{C_i} I, \quad i \in \{1,2\} \\ V &= V_{oc}(SOC) - R_s I - \sum_{i=1}^{2} V_i, \end{aligned} \tag{5}$$

where C_b represents the estimated capacity of the cell. Parameters R_s, R_1, R_2, C_1 and C_2 are estimated using pulse tests described in [17]. As these parameters are functions of temperature and SOC, a two dimensional look-up table is used to schedule the model parameters [18]. Figures 5(b) and (c) present a comparison between measured and simulated battery terminal voltages using the current profile employed in Fig. 4. The electrical submodel is validated independently using measured temperatures as shown in Fig. 5(a). It is observed that the error in the simulated voltage is less than 5% of the total variation in terminal voltage.

4 POWER CAPABILITY ESTIMATION METHOD

In this section, a computationally simple but effective method to estimate power capability is described. In estimating power capability, the following factors are considered

1. The thermal and electrical dynamics of a lithium-ion cell are intrinsically coupled. For a constant current, any arbitrary increase in cell temperatures will cause reduced internal losses, and subsequently generate less heat.
2. The rate of change of internal resistance with respect to temperature decreases with increasing temperatures.
3. Over a reasonably short horizon, the temperature increase can be assumed to be bounded and similar arguments can be made for the change in the electrical quantity, SOC.

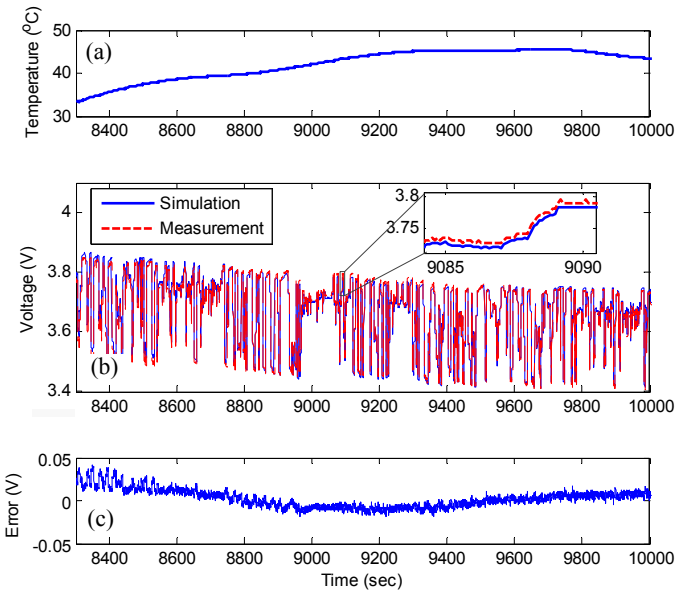

Figure 5. VALIDATION OF THE ELECTRICAL MODEL AND ITS PERFORMANCE UNDER VARYING TEMPERATURES: (a) TEMPERATURE; (b) VOLTAGE; (c) VOLTAGE ERROR

The above statements are valid insofar as the temperature of the cell does not exceed the threshold temperature at which thermal runaway is initiated [18, 19]. Since thermal dynamics are much slower than electrical dynamics, it follows that over a short horizon, in estimating power capability, considering electrical and thermal constraints independently yield conservative estimates. As a consequence, the thermal and electrical constraint problems are addressed separately.

To solve each constraint problem, the Algebraic Propagation (AP) method is utilized. The AP method, based on iteration and inversion of a dynamic model, allows us to estimate the maximal value of input ensuring that no constraints are violated.

Consider a linear discrete-time model whose dynamics is described by the following set of difference equations

$$\begin{aligned} x_{k+1} &= Ax_k + Bu_k + E \\ y_k &= Cx_k + Du_k + F \end{aligned} \tag{6}$$

where system matrices are denoted by A, B, C, D, E and F and are obtained through linearization and discretization processes around the operating point (x_o, u_o) at each sampling time. Following this notation, the linearized system matrices of the electrical and thermal models are denoted with superscripts or subscripts of e and θ respectively. For example, the discrete state transition matrix of the thermal model is denoted by A_θ.

For a constant input $\bar{u}$, the state x and output y after N future steps are written as

$$x_{k+N} = A^N x_k + \sum_{i=0}^{N-1} A^i B\bar{u} + \sum_{i=0}^{N-1} A^i E,$$
$$y_{k+N} = Cx_{k+N} + D\bar{u} + F. \tag{7}$$

Therefore, at any instant k, the maximum permissable input that does not violate a constraint $\bar{y}$ on the output y in N future steps is determined by

$$\bar{u} = \left(\sum_{i=0}^{N-1} CA^i B + D\right)^{-1} \left(\bar{y} - CA^N x_k - \sum_{i=0}^{N-1} CA^i E - F\right) \tag{8}$$

Equation (8) will be used to determine the maximal value of current accounting for thermal and electrical constraints in the following sections.

4.1 Active Thermal Constraints

The thermal dynamics in discrete time domain with a sampling period Δt can be captured by the following equation:

$$x_{\theta,k+1} = A_\theta x_{\theta,k} + v_k,$$
$$y_{\theta,k} = x_{\theta,k}, \tag{9}$$

where $A_\theta = 1 + \alpha\Delta t$. The virtual input, v, is defined as

$$v_k = \Delta t(\beta_k x_{\theta,k} u_k + \gamma_k u_k^2 + \eta_k). \tag{10}$$

Then, the maximum of the virtual input, $\bar{v}_k$, described by considering the maximum operating temperature, $\overline{T}$, is obtained from the following equation.

$$\bar{v}_k = \left(\sum_{i=0}^{N-1} C_\theta A_\theta^i\right)^{-1} \left(\overline{T} - C_\theta A_\theta^N x_{\theta,k}\right). \tag{11}$$

When the maximal value of current is less than 4C and the prediction period is less than 10 seconds, the SOC and temperature of the battery do not change significantly over the prediction horizon. Thus, it is reasonable to assume that the heat generation due to entropy change is constant over the prediction horizon, that is, $\beta_{j|k} x_{\theta,j|k} \approx \beta_k x_{\theta,k}$ for $j = k, k+1, \ldots, k+N$. This approximation makes it easy to handle the nonlinearity in the expression of heat generation rate using a quadratic term γu_k^2.

By substituting Eq. (11) into Eq. (10), the maximum permissible currents during battery discharge and charge are determined respectively by following equations

$$I_{max,k}^{\theta,\mathrm{dch}} = \frac{-\overline{\beta}_k + \sqrt{\overline{\beta}_k^2 - 4\gamma_k(\eta_k - \bar{v}_k/\Delta t)}}{2\gamma_k}, \tag{12}$$

$$I_{max,k}^{\theta,\mathrm{chg}} = \frac{-\overline{\beta}_k - \sqrt{\overline{\beta}_k^2 - 4\gamma_k(\eta_k - \bar{v}_k/\Delta t)}}{2\gamma_k}, \tag{13}$$

where $\overline{\beta}_k = \beta_k x_{\theta,k}$. Superscripts dch and chg present battery discharge and charge respectively.

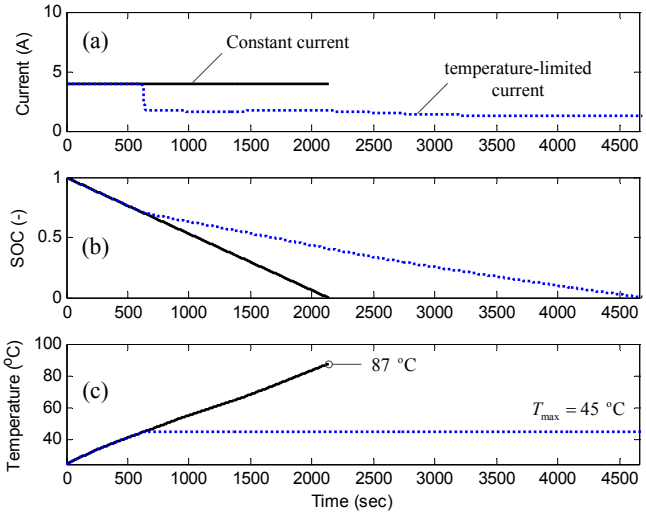

Figure 6. PERFORMANCE OF CURRENT LIMITING FOR TEMPERATURE CONTROL DURING CONSTANT CURRENT OPERATION AT 25^{o}C AMBIENT TEMPERATURE AND NATURAL CONVECTION (6 W/m^2/K): (a) CURRENT; (b) SOC; (c) TEMPERATURE

To investigate the efficacy of Eqs. (12) and (13) in controlling temperature, a simulation study is conducted. In the simulation, the sampling frequency is set at 10 Hz with a 100 sample prediction horizon. Figures 6(a)–(c) show the current drawn from the the cell, the corresponding SOC and cell temperature profiles. It is noted that the cell temperature increases up to 87^{o}C without limiting current rate. On the other hand, the cell temperature remains well around the designated maximal operating temperature of 45^{o}C when current is limited. Due to temperature-constrained current, as shown in Fig. 6(c), the completion time increases from 2133 seconds to 4687 seconds.

4.2 Active Electrical Constraints

The electrical dynamics in discrete time domain can be expressed as

$$x_{e,k+1} = A_e x_{e,k} + B_e u_k,$$
$$y_{e,k} = C_e x_{e,k} + D_e u_k + F_e, \tag{14}$$

where the state and output are defined as $x_e = [SOC \;\; V_1 \;\; V_2]^T$ and $y_e = [SOC \;\; V]^T$ respectively. System matrices A_e, B_e, C_e, D_e and F_e are calculated by

$$A_e = \begin{bmatrix} 1 & 0 & 0 \\ 0 & e^{\frac{-\Delta t}{R_1 C_1}} & 0 \\ 0 & 0 & e^{\frac{-\Delta t}{R_2 C_2}} \end{bmatrix}, B_e = \begin{bmatrix} -\frac{\Delta t}{C_b} \\ R_1\left(1 - e^{\frac{-\Delta t}{R_1 C_1}}\right) \\ R_2\left(1 - e^{\frac{-\Delta t}{R_2 C_2}}\right) \end{bmatrix},$$

$$C_e = \begin{bmatrix} 1 & 0 & 0 \\ \left.\frac{\partial V_{oc}}{\partial SOC}\right|_{SOC_0} & -1 & -1 \end{bmatrix}, D_e = \begin{bmatrix} 0 \\ -R_s \end{bmatrix},$$

$$F_e = \begin{bmatrix} 0 \\ V_{oc}(SOC_0) - \left.\frac{\partial V_{oc}}{\partial SOC}\right|_{SOC_0} SOC_0 \end{bmatrix},$$

where SOC_0 is the battery SOC at operating point about which the system is linearized.

By applying Eq. (8), the maximum permissible current accounting for electrical constraints such as SOC and voltage limits, $\overline{SOC}$ and $\overline{V}$, is determined respectively by using Eqs. (15) and (16).

$$I^{e,\overline{SOC}}_{max,k} = \left(\sum_{i=0}^{N-1} C_{e1} A_e^i B_e + D_{e1}\right)^{-1} \left(\overline{SOC} - C_{e1} A_e^N x_{e,k} - F_{e1}\right) \quad (15)$$

$$I^{e,\overline{V}}_{max,k} = \left(\sum_{i=0}^{N-1} C_{e2} A_e^i B_e + D_{e2}\right)^{-1} \left(\overline{V} - C_{e2} A_e^N x_{e,k} - F_{e2}\right) \quad (16)$$

where subscripts 1 and 2 denote the row indices of system matrices corresponding to SOC and terminal voltage respectively. The overall maximum permissible current is determined by comparing Eqs. (12), (15), (13), and (16).

4.3 Power Capability Estimation

The power capability accounting for all constraints is estimated by the product of the the maximum allowable current and terminal voltage. Maximum discharge and charge currents accounting for all constraints are calculated with

$$I^{\text{dch}}_{max,k} = \min\{I^{e,SOC_{min}}_{max,k}, I^{e,V_{min}}_{max,k}, I^{\theta,\text{dch}}_{max,k}\} \quad (17)$$

$$I^{\text{chg}}_{max,k} = \max\{I^{e,SOC_{max}}_{max,k}, I^{e,V_{max}}_{max,k}, I^{\theta,\text{chg}}_{max,k}\} \quad (18)$$

It is noteworthy that Eqs. (17) and (18) can be considered as general solutions that can be made specific to the load governor/regulator problem by choosing an appropriate prediction horizon and sampling frequency.

Therefore, the maximum power capability of the battery $P^q_{max,k}$, $q \in \{\text{dch,chg}\}$ is obtained as follows

$$P^q_{max,k} = I^q_{max,k} \cdot V^q_{k+N|k}, \quad (19)$$

where the terminal voltage after N future sample steps $V^q_{k+N|k}$ is calculated with

$$V^q_{k+N|k} = V_{oc}\left(SOC_k - \frac{I^q_{max,k} N\Delta t}{C_b}\right) - I^q_{max,k} R_s - \sum_{i=1}^{2}\left(e^{\frac{-N\Delta t}{R_i C_i}} V_{i,k} + I^q_{max,k} R_i \left(1 - e^{\frac{-N\Delta t}{R_i C_i}}\right)\right). \quad (20)$$

5 SIMULATION RESULTS

In this section, we investigate the performance of the proposed model-based power capability estimation method through a battery simulation with a prediction horizon of 10 seconds and a 10 Hz sampling frequency. Figures 7(b)–(e) show the estimated power capabilities and actual power drawn from the battery, corresponding terminal voltage, battery temperature and SOC profiles during repeated discharge duty cycles seen from Fig. 7(a). The ambient temperature and convection coefficient are assumed to be 30^oC and 6 W/m^2/K respectively. The electrical and thermal constraints are summarized in Table 1.

It is noted that all constraints are inactive initially, that is, the battery voltage, temperature and SOC do not exceed V_{min}, T_{max}, SOC_{min} respectively. Hence, the battery can provide the power requested up to 4705 second until the voltage constraint is violated. As the power is drawn from the battery, the battery SOC is reduced as seen from Fig. 7(e). Due to the corresponding decrease in open circuit voltage and voltage drop caused by internal resistances, the power is limited by the voltage-constrained power capability so that the terminal voltage is higher than the minimum limit of 3.2 V as shown in Fig. 7(c) from 4705 to 5740 second.

As the cell temperature approaches to the maximum temperature limit, the power capability is determined by the maximum temperature limit. Hence, as illustrated in 7(d), the battery temperature remains below 45^oC until SOC constraint becomes active. This performance highlights that the proposed method is capable of estimating power capability accounting for thermal and electrical constraints and thus safe and reliable operation of the battery is achievable.

Table 1. THERMAL AND ELECTRICAL CONSTRAINTS

Constraint	Unit	Value
Max. Temperature	^{o}C	45
Min. Voltage	V	3.2
Min. SOC	-	0.05

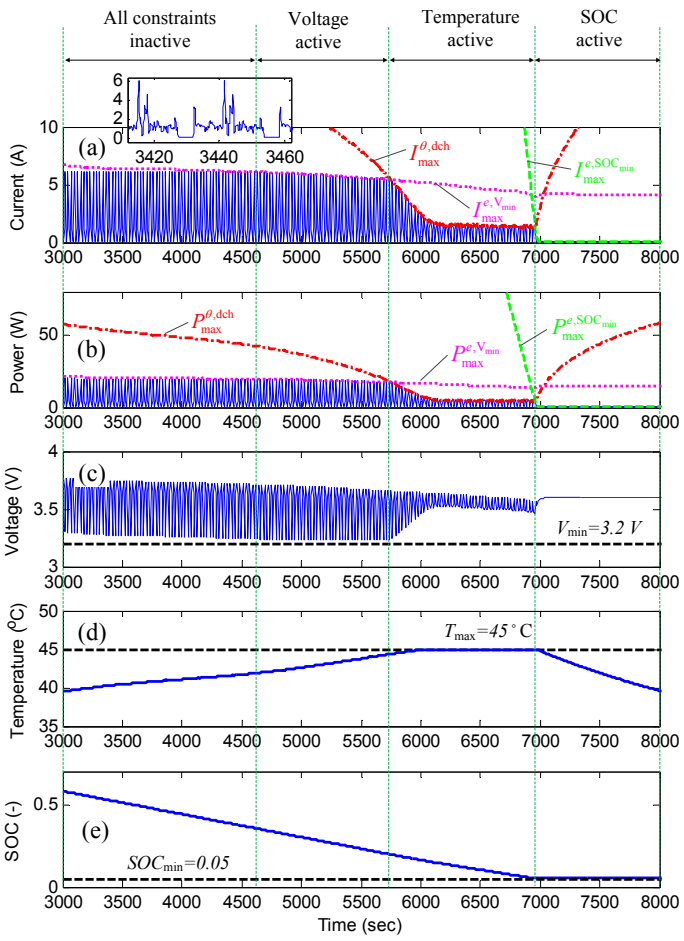

Figure 7. PERFORMANCE OF POWER CAPABILITY ESTIMATION METHOD DURING REPEATED OPERATIONS AT 30^{o}C AMBIENT TEMPERATURE AND NATURAL CONVECTION (6 W/m^2/K): (a) CURRENT; (b) POWER; (c) VOLTAGE; (d) TEMPERATURE; (e) SOC

6 CONCLUSION

In this paper a method to estimate battery power limits accounting for both electrical and thermal constraints is presented. The method relies on an electro-thermal model for the electrical and thermal dynamic behaviors. Further, a method to parameterize the lumped thermal model that includes entopic heat generation as well as joule heating is presented and discussed. Under the assumptions of short prediction horizons, the power capability estimation problem is broken into a current limiting problem under two weakly coupled constraints– thermal and electrical. A computationally efficient algorithm is proposed that is able to exploit the weakly nonlinear nature of the thermal dynamics.

A future extension of this work could explore the impact of the assumption of weak coupling between thermal and electrical dynamics as prediction horizon increases on the estimation of power capability. In addition, the proposed method could be scaled to the pack level and applied to automotive and robotic systems.

REFERENCES

[1] Pistoia, G., 2009. *Battery operated devices and systems: From portable electronics to industrial products*. Elsevier Science Limited.

[2] Shim, J., Kostecki, R., Richardson, T., Song, X., and Striebel, K., 2002. "Electrochemical analysis for cycle performance and capacity fading of a lithium-ion battery cycled at elevated temperature". *Journal of Power Sources,* **112**(1), pp. 222 – 230.

[3] Tobishima, S., and Yamaki, J., 1999. "A consideration of lithium cell safety". *Journal of Power Sources,* **81-82**(0), pp. 882 – 886.

[4] Spotnitz, R., and Franklin, J., 2003. "Abuse behavior of high-power, lithium-ion cells". *Journal of Power Sources,* **113**(1), pp. 81–100.

[5] Andrea, D., 2010. *Battery management systems for large lithium-ion battery packs*. Artech House Publishers.

[6] Plett, G., 2004. "High-performance battery-pack power estimation using a dynamic cell model". *IEEE Transactions on Vehicular Technology,* **53**(5), Sept., pp. 1586 – 1593.

[7] Anderson, R. D., Zhao, Y., Wang, X., Yang, X. G., and Li, Y., 2012. "Real time battery power capability estimation". In Proceedings of the American Control Conference, pp. 592–597.

[8] Xiong, R., He, H., Sun, F., Liu, X., and Liu, Z., 2013. "Model-based state of charge and peak power capability joint estimation of lithium-ion battery in plug-in hybrid electric vehicles". *Journal of Power Sources,* **229**(0), pp. 159 – 169.

[9] Jeon, D. H., and Baek, S. M., 2011. "Thermal modeling of cylindrical lithium ion battery during discharge cycle". *Energy Conversion and Management,* **52**(8-9), pp. 2973–2981.

[10] Pendergast, D. R., DeMauro, E. P., Fletcher, M., Stimson, E., and Mollendorf, J. C., 2011. "A rechargeable lithium-ion battery module for underwater use". *Journal of Power Sources,* **196**(2), pp. 793–800.

[11] Maleki, H., Hallaj, S. A., Selman, J. R., Dinwiddie, R. B., and Wang, H., 1999. "Thermal properties of lithium-ion battery and components". *Journal of The Electrochemical Society,* **146**(3), pp. 947–954.

[12] Chen, S., Wan, C., and Wang, Y., 2005. "Thermal analysis of lithium-ion batteries". *Journal of Power Sources,* **140**(1), pp. 111–124.

[13] Onda, K., Ohshima, T., Nakayama, M., Fukuda, K., and Araki, T., 2006. "Thermal behavior of small lithium-ion battery during rapid charge and discharge cycles". *Journal of Power Sources,* **158**(1), pp. 535–542.

[14] Takano, K., Saito, Y., Kanari, K., Nozaki, K., Kato, K., Negishi, A., and Kato, T., 2002. "Entropy change in lithium ion cells on charge and discharge". *Journal of Applied Electrochemistry,* **32**, pp. 251–258.

[15] Viswanathan, V. V., Choi, D., Wang, D., Xu, W., Towne, S., Williford, R. E., Zhang, J.-G., Liu, J., and Yang, Z., 2010.

"Effect of entropy change of lithium intercalation in cathodes and anodes on li-ion battery thermal management". *Journal of Power Sources,* **195**(11), pp. 3720 – 3729.

[16] Kim, Y., Siegel, J. B., and Stefanopoulou, A. G., 2013. "A computationally efficient thermal model of cylindrical battery cells for the estimation of radially distributed temperatures". In American Control Conference, Accepted.

[17] Gao, L., Liu, S., and Dougal, R. A., 2002. "Dynamic lithium-ion battery model for system simulation". *IEEE Transactions on Components and Packaging Technologies,* **25**(3), pp. 495–505.

[18] Perez, H. E., Siegel, J. B., Lin, X., Ding, Y., and Castanier, M. P., 2012. "Parameterization and validation of an integrated electro-thermal LFP battery model". In ASME Dynamic Systems Control Conference, Oct 17-19.

[19] Hammami, A., Raymond, N., and Armand, M., 2003. "Lithium-ion batteries: Runaway risk of forming toxic compounds". *Nature,* **424**(6949), pp. 635–636.